Titanium Dioxide Coatings Sprayed by a Water-Stabilized Plasma Gun (WSP) with Argon and Nitrogen as the Powder Feeding Gas: Differences in Structural, Mechanical and Photocatalytic Behavior

P. Ctibor, Z. Pala, J. Sedláček, V. Štengl, I. Píš, T. Zahoranová & V. Nehasil

Journal of Thermal Spray Technology

ISSN 1059-9630
Volume 21
Combined 3-4

J Therm Spray Tech (2012) 21:425-434
DOI 10.1007/s11666-012-9747-0

Springer

JTTEE5 21:425–434
DOI: 10.1007/s11666-012-9747-0
1059-9630/$19.00 © ASM International

Titanium Dioxide Coatings Sprayed by a Water-Stabilized Plasma Gun (WSP) with Argon and Nitrogen as the Powder Feeding Gas: Differences in Structural, Mechanical and Photocatalytic Behavior

P. Ctibor, Z. Pala, J. Sedláček, V. Štengl, I. Píš, T. Zahoranová, and V. Nehasil

(Submitted September 9, 2011; in revised form January 12, 2012)

Titanium dioxide coatings were sprayed by a water-stabilized plasma gun to form robust self-supporting bodies with a photocatalytically active surface. Agglomerated nanometric powder was used as a feedstock. In one case argon was used as a powder-feeding as well as coating-cooling gas whereas in the other case nitrogen was used. Stainless steel was used as a substrate and the coatings were released after the cooling. Over one millimeter thick self-supporting bodies were studied by XRD, HR-TEM, XPS, Raman spectroscopy, UV-VIS spectrophotometry and photocatalytic tests. Selected tests were done at the surface as well as at the bottom side representing the contact surface with the substrate during the spray process. Porosity was studied by image analysis on polished cross sections where also microhardness was measured. The dominant phase present in the sprayed samples was rutile, whereas anatase was only a minor component. The hydrogen content in the nitrogen-assisted coating was higher, but the character of the optical absorption edge remained the same for both samples. Photoelectron spectroscopy revealed differences in the character of the O1s peak between both samples. The photocatalytic activity was tested by decomposition of acetone at UV illumination, whereas also the end products—CO and CO_2—were monitored. The nitrogen-assisted coating was revealed as a more efficient photocatalyst. Certain aspects of a thermal post-treatment on the coatings are discussed as well. Color and electrical conductivity are markedly changed at annealing at 760 °C, whereas only very small changes of the as-sprayed coating character correspond to annealing at 500 °C.

Keywords bandgap, photocatalysis, resistivity, spectroscopy, TiO_2

1. Introduction

Titanium dioxide (TiO_2) has many applications, namely in photo-catalytic, dielectric and optical-coating components. Preparation of the catalysts coated as films make it possible to overcome disadvantages associated with using ultrafine powder catalytic substances and by this way to extend industrial applications, such as e.g., antibacterial ceramic tile and self-cleaning glass. Titanium dioxide is one of the most important photocatalysts used for such applications. Its photocatalytic activity depends on various parameters such as crystalline phases, particle size, morphology and heat treating conditions (Ref 1-3). Coating technology such as vapor deposition, sol-gel and thermal spray are effective methods to obtain nanostructured TiO_2 coatings starting from nanopowders.

Titanium dioxide begins to lose oxygen at a temperature above 1600 °C in reductive as well as neutral atmospheres. The partial pressure of oxygen required to reduce TiO_2 to Ti_2O_3, Ti_3O_5 or Ti_4O_7 is of the order of 10^{-5} Pa at around 2000 °C. Oxygen-deficient phases of TiO_2 (especially Ti_3O_5, Ti_6O_{11}) are sometimes observed in the coatings by XRD, especially when the feedstock is an agglomerated titania nanopowder (Ref 4). In thermally sprayed TiO_2 the result of interaction of the initial (stoichiometric) TiO_2 powder with plasma is formation of reduced TiO_x. The redox reaction between the orthorhombic titanium oxide TiO_x and the rutile TiO_2 is reversible at 950 °C (Ref 5). An energetically favorable coupled system of rutile with suboxide phases (Ref 6) will

This article is an invited paper selected from presentations at the 2011 International Thermal Spray Conference and has been expanded from the original presentation. It is simultaneously published in *Thermal Spray 2011: Proceedings of the International Thermal Spray Conference*, Hamburg, Germany, September 27-29, 2011, Basil R. Marple, Arvind Agarwal, Margaret M. Hyland, Yuk-Chiu Lau, Chang-Jiu Li, Rogerio S. Lima, and André McDonald, Ed., ASM International, Materials Park, OH, 2011.

P. Ctibor and **Z. Pala**, Institute of Plasma Physics, ASCR, Za Slovankou 3, 182 00 Praha 8, Czech Republic; **J. Sedláček**, Department of Electrotechnology, Faculty of Electrical Engineering, Czech Technical University, Technická 2, Praha 6, Czech Republic; **V. Štengl**, Institute of Inorganic Chemistry, ASCR, Husinec-Rez 250 68, Czech Republic; and **I. Píš, T. Zahoranová,** and **V. Nehasil**, Department of Surface and Plasma Science, Faculty of Mathematics and Physics, Charles University, V Holesovickach 2, 180 00 Praha 8, Czech Republic. Contact e-mail: ctibor@ipp.cas.cz.

thus show unique features by providing a great enhancement of the photocatalytic activity. This effect may be at the heart of the high photocatalytic activity of plasma-sprayed coatings. Plasma sprayed coatings with reasonable potential for various photocatalytic applications have been reported. Coatings have been sprayed on conventional as well as special substrates such as foamed aluminum (Ref 7) or PET plates (Ref 8). In other cases, various approaches for an enhancement of the photoactivity were tested—spraying of nano-structured powders (Ref 4, 9), a post-deposition treatment (Ref 10), HVOF spraying (Ref 11) or the suspension plasma spray technique (Ref 12). The origin of a non-stoichiometric and oxygen deficient lattice in rutile TiO_2 at plasma spraying is due to the formation of structural defects.

The goal of the present paper is to compare the structural character and coating photochemical properties when an agglomerated, originally nanometric, TiO_2 powder (Ref 13) is deposited by water-stabilized plasma (WSP) spraying. WSP is a technique with a markedly higher powder processing rate of the TiO_2 material compared to conventional plasma spray torches. However, this fact is associated with higher plasma temperature, enthalpy and features like the presence of ionized oxygen in the plasma. For these reasons the applicability window for this device concerning the photocatalytic coatings may be different compared to other thermal spray guns.

In the current report, Ar and N_2 were compared as the gases used for the powder feeding and substrate cooling simultaneously. It will be demonstrated that because of a different reactivity of both addressed gases with TiO_2, selected aspects of the resulting coatings differ remarkably.

2. Experimental

2.1 Feedstock Powder and Spray Process

The TiO_2 powder (Ref 13) (Altair Nanomaterials Inc., Reno, NV, USA) was prepared from a nanometric powder by agglomeration. The fraction from 45 to 150 μm in size was utilized for spray experiments at various processing conditions. Samples were produced using the WSP spray system WSP® 500 (Institute of Plasma Physics, Prague, Czech Republic). The powder was fed in by compressed air through two injectors and the thickness of the produced coatings was about 1.5 mm. Stainless steel coupons were used as substrates. Some of the coatings were then stripped-off for further characterizations. The spray parameters, see Table 1, were fixed for both spray rounds and the only difference was in the gas used. Argon was used in one spray round as a powder feeding gas. A pressure of 2.5 bar and a flow rate of 3.25 slpm were employed. Ar was used also for substrate cooling and cooling the just deposited coating. The cooling tube was installed on the robot and after each pass it copied the movement pattern of the spray gun over the substrate. The temperature was monitored by a two-color pyrometer, not to exceed 250 °C. In the next spray experiment, exactly the same procedure was repeated with nitrogen in both functions.

Table 1 Parameters used for spraying

Parameter	Value
Feeding distance FD, mm	120
Spray distance SD, mm	400
Feeding nozzle diameter, mm	3
Torch power, kW	150

2.2 Characterization Techniques

The porosity was studied by optical microscopy on polished cross sections. The micrographs were taken with a CCD camera and processed using an image analysis (IA) software (Lucia G, Laboratory Imaging, Czech Rep.). Ten images of microstructures taken from various areas of a cross section for each sample were analyzed. The used magnification was 250 in all cases. For a better description of the porosity certain additional criteria were introduced (Ref 13).

The microstructure of the coatings was studied also by a High Resolution Transmission Electron Microscope (HR-TEM) Jeol JEM 3010.

The content of hydrogen was measured by the LECO technique (Leco RH 404 apparatus). This technique is based on melting of a small amount of the material whereas a spectral analysis of the melt provides a quantitative evaluation of the content of low-concentration admixtures. The quantity of analyzed material was 1 g for each sample.

X-ray diffraction (XRD) was performed on a SIEMENS D500™ theta-2theta Bragg-Brentano diffractometer, using cobalt K-α radiation, in order to gain information about the phases present within the feedstock powder and coatings.

The microhardness was measured by a Hanemann microhardness head (Zeiss, Germany) mounted on an optical microscope with a fixed load of 1 N and a Vickers indenter. Twenty indentations from various areas of a cross section for each sample were analyzed.

Raman spectroscopy was performed using a Lambda Solutions P1 apparatus—laser wavelength 785 nm, objective ×50, radiation power 250 mW, integration time 25 s.

X-ray photoelectron spectroscopy was carried out in an ultra-high vacuum chamber using an Omicron EA 125 multichannel hemispherical analyzer with Al K-α line (1486.6 eV) as a primary photon source. Ti 2p and O1s photoelectron peaks were recorded. In order to exclude the charging effects during the XPS experiments, the photoelectron binding energies (EB) were referenced to the Ti $2p_{3/2}$ peak of TiO_2, which was assumed to be positioned at the constant binding energy EB = 458.8 eV.

The diffuse reflectance was measured by UV-VIS-NIR scanning spectrophotometer (Shimadzu, Japan) with a multi-purpose large sample compartment, and the corresponding band-gap energy was estimated. The reflectance curves obtained between 200 and 2000 nm were then converted to absorbance and recalculated (Ref 14) to a bandgap energy E_{bg}.

The kinetics of the photocatalytic degradation of gaseous acetone was measured by using a self-constructed

stainless steel photoreactor with a fluorescent lamp Narva LT8WT8/073BLB, a black lamp with 365 nm wavelength and input power 8 W (light intensity 6.3 mW/cm^2). The gas concentration was measured with a quadrupole mass spectrometer JEOL JMS-Q100GC and gas chromatograph Agilent 6890N. A high-resolution gas chromatography column (19091P-QO4, J&W Scientific) was used. The sample from the reactor was taken via a sampling valve at a time interval of 2 h. The reactor of total volume of 3.5 l was filled with oxygen at a flow rate of 1 l per minute.

Annealing of plasma sprayed deposits was carried out on the samples released from the metallic substrate (free-standing body) in a laboratory furnace at different temperatures in air atmosphere. The heating as well as cooling speed was 7 °C per minute and the dwell time was 30 min in all cases. The annealing temperatures were selected with respect to re-oxidation temperature, which according to our preliminary tests was between 500 and 750 °C.

Electric resistance was measured on as-sprayed as well as annealed samples with a special resistivity adapter—Keithley model 6105. The electric field was applied from a regulated high-voltage source and the values read by a multi-purpose electrometer (617C, Keithley Instruments, USA). The magnitude of the applied voltage was 100 ± 2 V DC. Volume resistivity was calculated from the measured resistance and specimen dimensions. On average, five specimens were measured and the mean values calculated.

Dielectric measurements were performed on the 760 °C-annealed samples released from the metallic substrate (free-standing body). The as-sprayed and also the 500 °C-annealed samples were too conductive for these measurements. The surface of the samples was ground to eliminate surface roughness. Layers of aluminum as thin film electrodes were sputtered in a reduced pressure on both sides of each sample. The electric field was applied parallel to the spraying direction (i.e., perpendicular to the substrate surface). Capacity was measured in the frequency range from 180 Hz to 1 MHz using a programmable impedance analyzer model PM6306 (Fluke, the Netherlands). Applied voltage was 1 V AC. Relative permittivity ε_r was calculated from measured capacities C_P and specimen dimensions since ε_r is directly proportional to C_P by the equation

$$C_P = \varepsilon_0 \times \varepsilon_r \times 1/k,$$

where $\varepsilon_0 = 8.854 \times 10^{-12}$ F m^{-1}; $1/k$ (m) is defined as the ratio between the surface and the thickness of the sample. This same arrangement and equipment was used for the loss tangent measurement at the same frequencies as capacity. Presented data represent averages from five samples.

3. Results and Discussion

3.1 Microstructure of Feedstock and Coatings

As-sprayed coatings exhibit typical lamellar microstructure with some pores and cracks, Fig. 1. Those voids are present in the nitrogen-assisted coating in slightly larger volume (porosity, in Table 2) and larger mean size (ED-pores in Table 2) as well as maximum size (ED_{max}-pores in Table 2). Minimal circularity is lower for the nitrogen-assisted coating, which indicates slightly flatter pores. We can summarize that all studied aspects of the porosity are worse in the nitrogen-assisted case.

According to the XRD analysis, 96 % of the feedstock was comprised of anatase; the rest was rutile. Detailed analysis of Ti/O ratio in the feedstock was done by EDX spot analysis. The average stoichiometry TiO_x of the individual particles was $x = 2.03 \pm 0.35$. The statement that as a rule, commercially available feedstock powders are sub-stoichiometric (Ref 15), was not confirmed in our case.

Figure 2 shows a HR-TEM image of the argon-assisted coating. Planar stacking faults are visible in the top part of the image—Ti_nO_{2n-1} consisting of rutile blocks which are infinite in two dimensions and finite in the third one (Ref

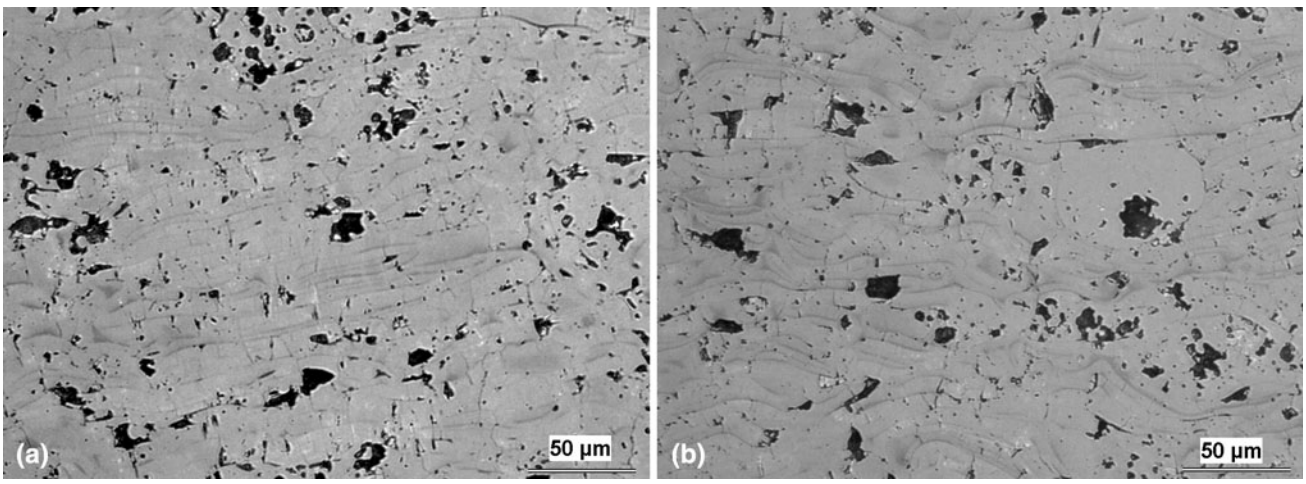

Fig. 1 Light micrograph of a polished cross section of the argon-assisted coating (a) and nitrogen-assisted coating (b)

16). Similar features were observed also for the nitrogen-assisted coating.

The analyses of XRD patterns measured on both sides of the coatings confirm that rutile is the dominant phase. Differences between the diffraction patterns measured on the surface sides belonging to both coatings are virtually non-existent; the only identified phase is rutile. However, diffraction patterns of both the bottom sides show the presence of anatase, most pronounced in the case of the nitrogen-assisted coating, as seen in Fig. 3.

The Raman spectra of both coatings are displayed in Fig. 4. The pattern with peaks at 440 cm^{-1} (E_g) and 610 cm^{-1} ($A1_g$) corresponds to the rutile phase of TiO_2 (Ref 17).

By Raman spectroscopy, the presence of TiO_2 in the anatase form has been identified—the peak at 143 cm^{-1} was observed in a TiO_2 film (Ref 18, 19) and at 147 cm^{-1} in the case of a coating (Ref 6). The broad multiple peak at approximately 255 cm^{-1} results from a second order process (Ref 17).

Hydrogen content in the nitrogen-assisted coating was higher (25.3 ppm) than in the argon-assisted coating (12.2 ppm). The presence of the interstitial N promotes the reduction of TiO_2. $TiO_{(2-x)}$ is chemically active and reacts more strongly with H from H_2O in the ambient air atmosphere.

Table 2 Image analysis of pores in the coatings

Sample	Porosity, %	ED, µm	ED_{max}, µm	Pores per mm^2	CIR_{min}
Ar-assis.	8.53	13.55	19.84	171	0.0946
N-assis.	9.39	14.75	26.38	183	0.0795

In Fig. 5(a) and (b) photoemission spectra of the TiO_2 feedstock powder, the nitrogen-assisted coating (bottom side), and the argon-assisted coating (surface side), are compared. The almost identical Ti 2p spectra revealed that the Ti element in the coatings mainly exists in the chemical state Ti^{4+}. The oxygen O1s spectra (Fig. 5b), on the other hand, showed distinct differences between the three samples.

The main peak at 530 eV, common for all samples, corresponds to the oxygen in the crystal lattice. A second peak at the energy of 532.3 eV appeared on the coatings and is assigned to surface OH groups (Ref 20, 21), which play an important role in the photocatalytic activity.

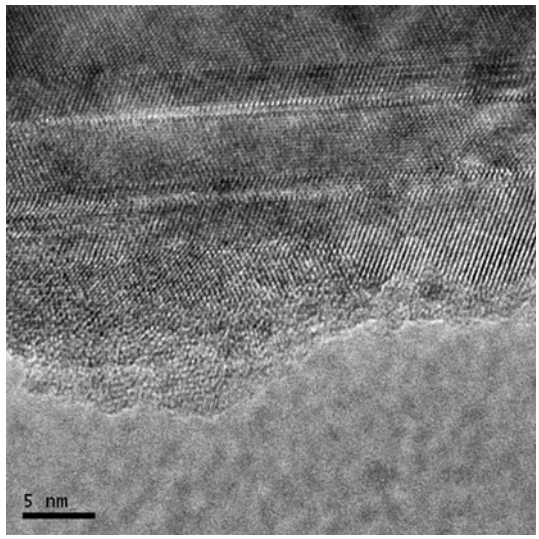

Fig. 2 HR-TEM micrograph of the argon-assisted coating

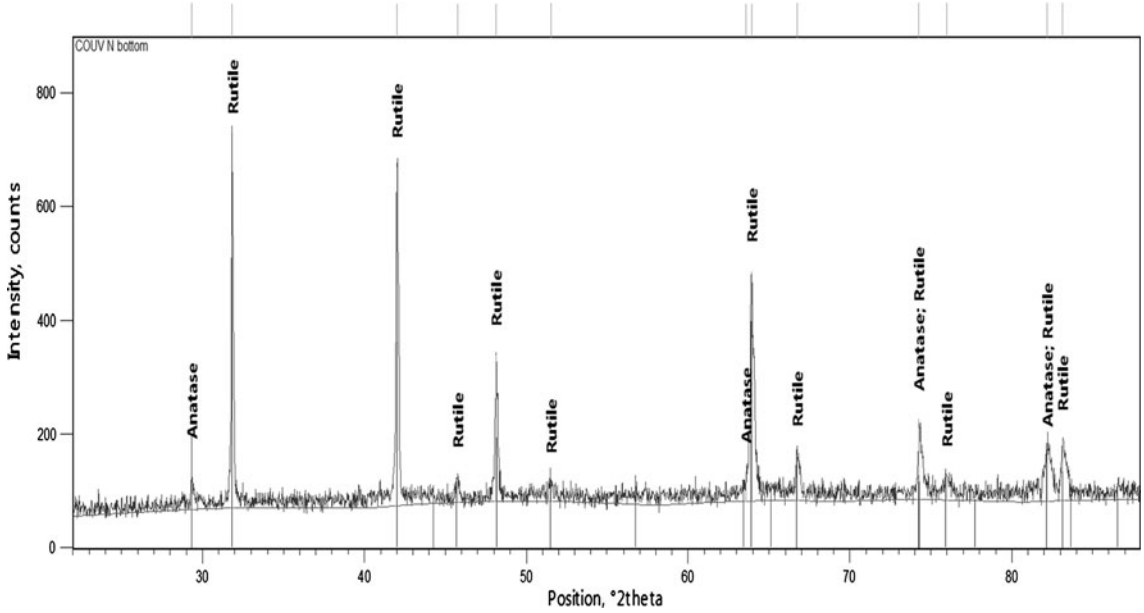

Fig. 3 XRD pattern of the nitrogen-assisted coating, bottom surface

Figure 5(c) and (d) display XPS spectra of the TiO_2-nitrogen-assisted coating (bottom side). In contrast to the other samples, the Ti 2p spectrum revealed a significant amount of Ti on the surface also in the Ti^{3+} (457.4 eV) and Ti^{2+} (456.0 eV) state (Ref 22), which indicates a presence of oxygen vacancies. The decomposition of the O1s spectrum into components was rather complicated because of the overlaps between oxygen peaks from TiO_2, Ti_2O_3 and TiO near 530 eV (Ref 22). Nevertheless, the O1s signal, broadened at higher binding energies, indicates the presence of OH groups also on this surface, with some chemisorbed water as well (Ref 23).

Figure 6 shows the nitrogen N1s spectra of the Ar-assisted coating (surface) and spectra of N-assisted coating, substrate-side as well as surface-side. The N 1s peak of the N-assisted coating substrate side has a maximum at 400.7 eV which corresponds to the nitrogen in the interstitial positions in TiO_2 (called also N-TiO_2) (Ref 24, 25).

The N1s peak of the N-assisted coating surface side has a maximum at 399.4 eV, which indicates the presence of nitrogen also in other chemical states. Correspondingly the full width at half maximum (FWHM) of this peak is 3.6 eV whereas the FWHM of the substrate side peak is about 2.2 eV. Taking into account the high area of the surface side peak the presence of NO_x, NH_x, NC_x molecules and also TiN on the surface of the N-assisted coating can be suggested.

Concerning the oxygen stoichiometry, based on XPS data where the element concentrations are influenced also by N and C, only a rough estimation can be done: the x in TiO_x on the surface of the N-assisted coating is twice

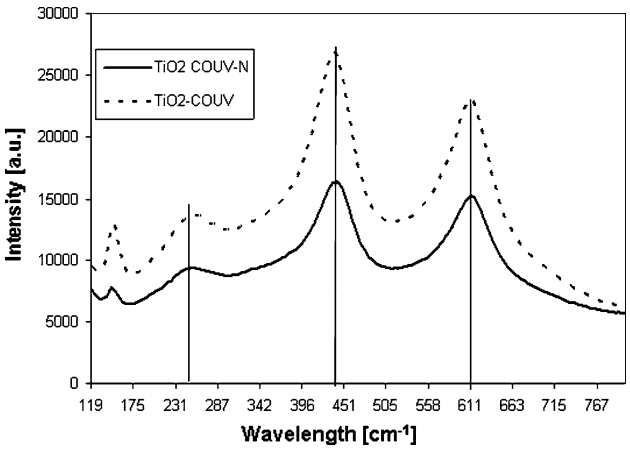

Fig. 4 Raman spectra of the argon (COUV) and nitrogen (COUV-N) assisted TiO_2 coatings

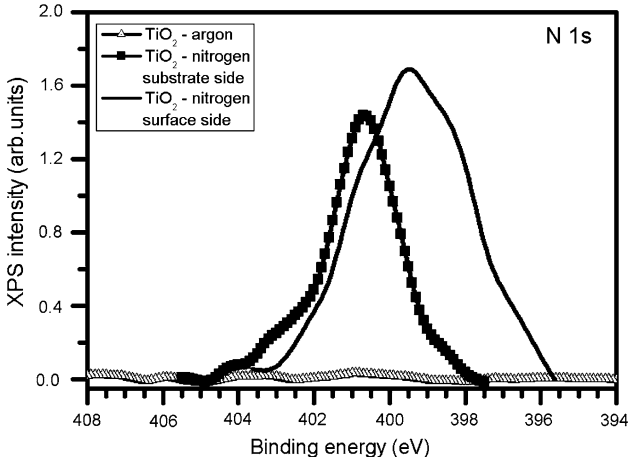

Fig. 6 Nitrogen N1s spectra of the Ar-assisted coating (surface) and spectra of N-assisted coating substrate—as well as surface-side

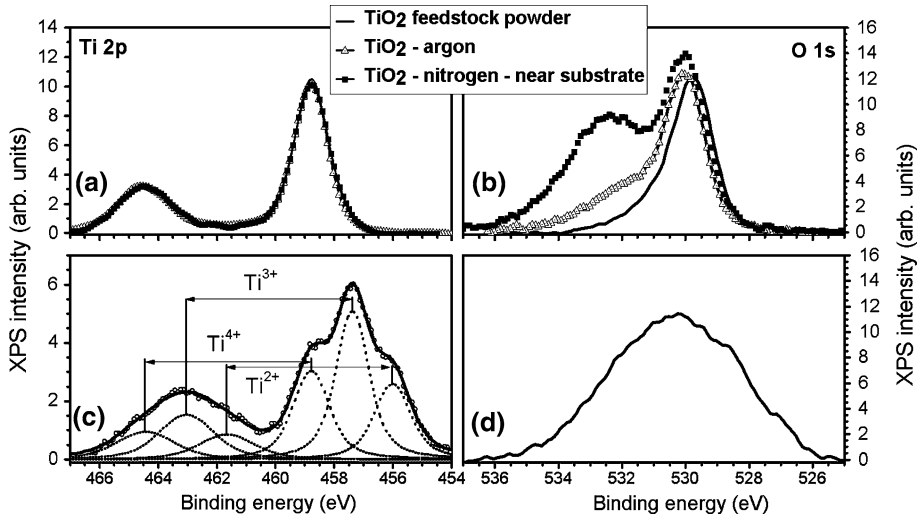

Fig. 5 Ti 2p (a) and O1s (b) XPS spectra of the feedstock powder (solid line), argon-assisted coating surface side (triangles) and nitrogen-assisted coating bottom side (squares). On the bottom, the Ti 2p (c) and O1s (d) spectra of the surface side of the nitrogen-assisted coating are displayed

Table 3 Microhardness of the coatings

Microhardness at 1 N	Mean value, GPa	SD, GPa
Ar-assisted—whole	9.46	1.31
N-assisted—near the surface	9.39	1.29
N-assisted—near the bottom side	9.54	1.34

lower than in all other cases (however, it is always lower than 2).

3.2 Mechanical Properties of Coatings

The microhardness was measured at 1 N; certain indents were made near the surface and a second half of indents near the interface with the substrate (bottom side), Table 3. The mean value from both such regions together is slightly higher for the argon-assisted coating, in agreement with the expectation based on the porosity character mentioned above. However, the difference is rather subtle and lies within a standard deviation, which is larger for the nitrogen-assisted coating. This fact is also associated with the porosity character. Interesting is that the difference between the microhardness near the bottom side and near the surface is higher for the nitrogen-assisted coating. This is associated with the chemically disordered character of this surface-faced side, as revealed by XPS. The existence of oxy-nitrides is well known in the Ti-based ceramics (Ref 26). However, in our coatings interstitial nitrogen, which is more prospective for photoactivity (Ref 27), is predominant.

3.3 Photochemical Behavior

The region that extends from the top of the filled valence band to the bottom of the vacant conduction band is called the band gap. The band gap energy of rutile is 3.0 eV (Ref 28) and of anatase 3.2 eV (Ref 29, 30). Therefore, surfaces where anatase and rutile are combined are in certain cases more efficient photocatalysts (Ref 31) than a single-phase TiO_2.

Our coatings contain on the surfaces only the rutile phase, whereas only the surface-side of the N-assisted coating contains both phase components—rutile and (minor) anatase. Both coatings have identical E_{bg} vs. $(\alpha \cdot E_{bg})^{1/2}$ plots, as shown in Fig. 7. The bandgap energy value [assuming indirect transition between valence and conduction band (Ref 32)] splits into two levels $E_{bg}(1)$ at 3.20 eV and $E_{bg}(2)$ at 2.30 eV. The main absorption edge at $E_{bg}(1)$ corresponds to non-stoichiometric TiO_2 with rutile as the main component and the secondary absorption edge at $E_{bg}(2)$ corresponds to an absorption tail of delocalized electronic states (Ref 5, 33) with low excitation energy. The higher value of $E_{bg}(1)$ vs. the nominal value for rutile (blue shift) occurs because of the vacancies, interstitial nitrogen atoms and stacking faults present in the coatings.

The photocatalytic degradation of acetone is depicted in Fig. 8(a). The kinetics of the concentration drop of acetone is similar for both samples. The curves are

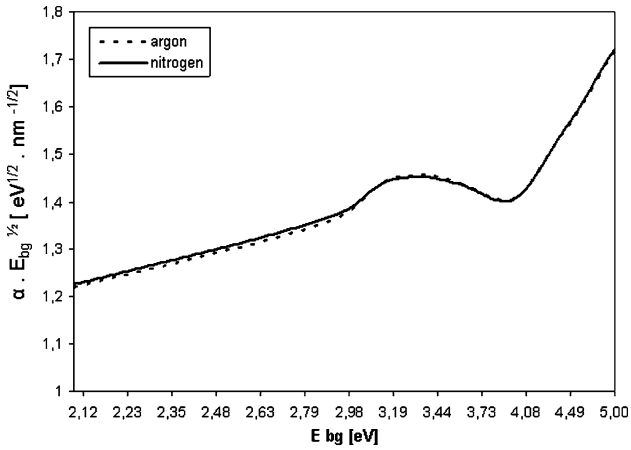

Fig. 7 Bandgap energy estimation for both coatings

displayed in comparison with the best and worst coatings tested by the authors—many dozens of samples sprayed from various TiO_2-based ceramics being included. The ''best coating'' represents a sample sprayed from rutile feedstock (air used as a feeding gas to diminish the TiO_2 reduction in the plasma) and the ''worst coating'' is a sample sprayed from alumina-40 wt. titania powder.

The major products of the acetone decomposition are carbon dioxide and carbon monoxide. Both of them have monotonous growth of concentration with time, see Fig. 8(b) and (c). Both coatings that are the focus of this paper occupy the medium zone of all kinetic graphs, far from the best and also from the worst samples mentioned in the previous paragraph.

The nitrogen-assisted coating promotes a faster decrease of acetone concentration and increase of CO and CO_2 concentrations. It can also be said that the nitrogen-assisted coating is a more efficient photocatalyst. The higher activity can be related to the higher porosity and thus higher surface area as well as to the higher amount of hydroxyl groups on the surface and interstitial nitrogen atoms.

The surface hydroxyl groups can act as the centers of photo-catalytic reactions. The combination of a photo-generated hole and the surface OH group results in the formation of the highly reactive OH radical bound to the surface (Ref 7, 20). Another reason could be found in the higher content of hydrogen (detected with LECO extraction analysis), which comes from the water vapor in the ambient air and in the coating is probably incorporated in the superficial OH-groups (detected by XPS).

3.4 Electrical Properties of the Annealed Coatings

Both as-sprayed coatings are electrically conductive, see Table 4. After annealing at 500 °C the volume resistivity further drops, with very low resistivity values due to annihilation of some defects like OH groups and other sources of a chemical disorder. The color of these samples is nearly identical with the as-sprayed coatings. After annealing at 760 °C the coatings became insulating and the color is now pale grey—cf. Table 4. These samples

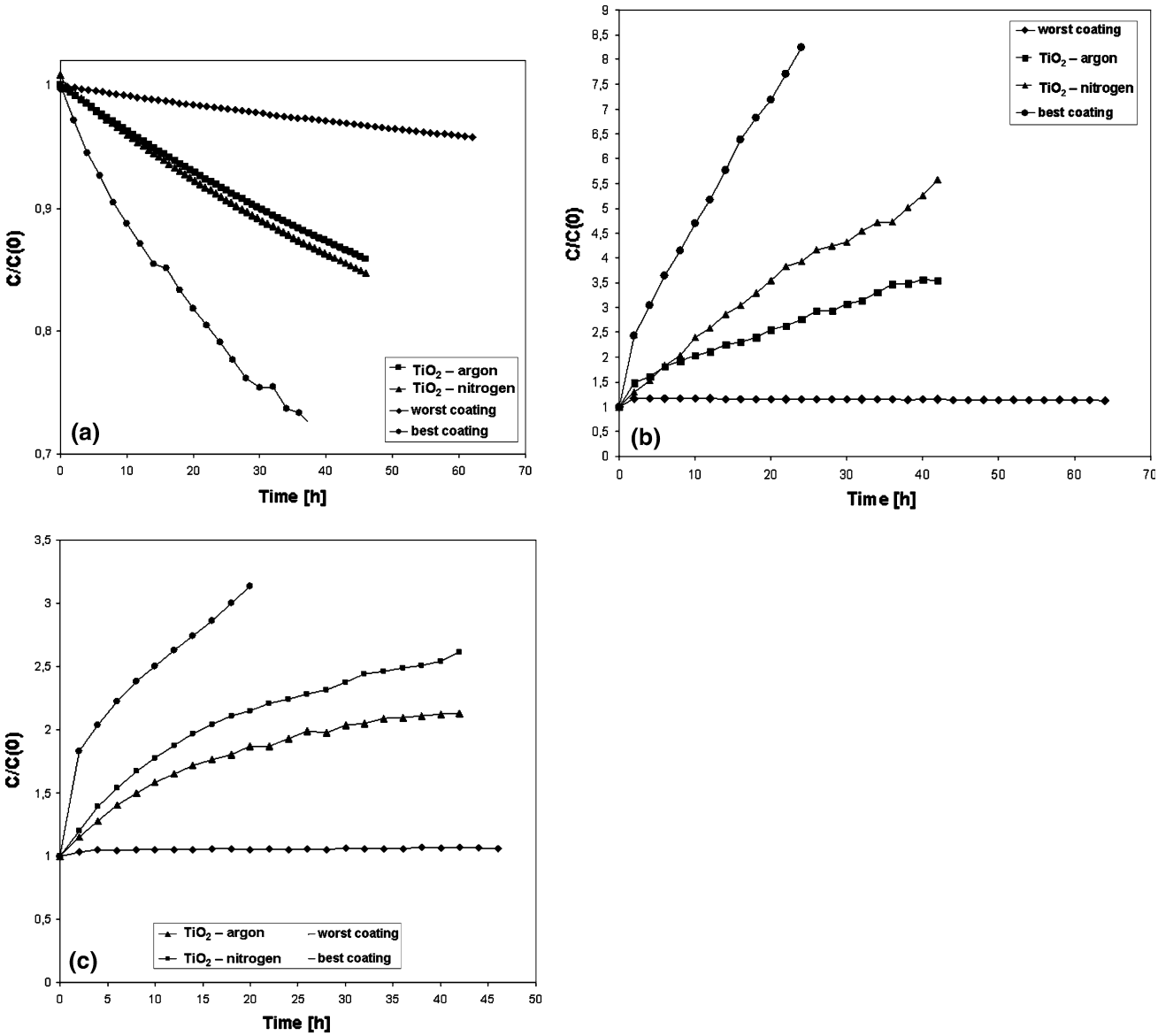

Fig. 8 Photocatalytic test: The kinetics of the concentration drop of acetone (a) and concentration growth of CO_2 (b) and CO (c)

Table 4 Volume resistivity of the coatings

Volume resistivity, Ωm	As-sprayed	Annealed 500 °C	Annealed 760 °C
Ar-assisted	1040	3.19	1.3×10^9
Surface color			
N-assisted	1140	1.26	4.1×10^8
Surface color			

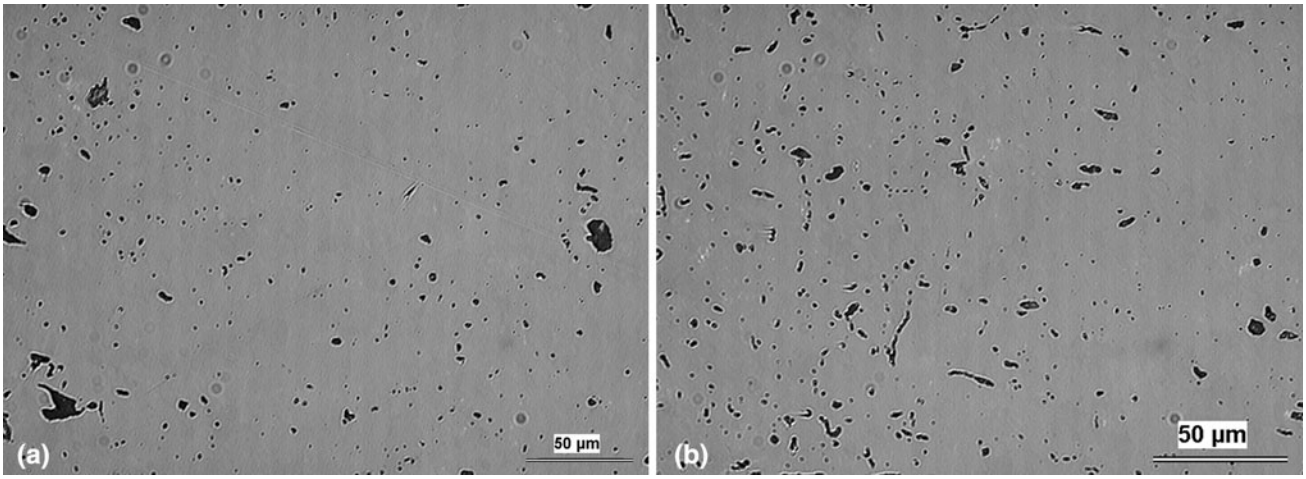

Fig. 9 Light micrograph of a polished cross section of the argon-assisted coating (a) and nitrogen -assisted coating (b), both after annealing to 760 °C

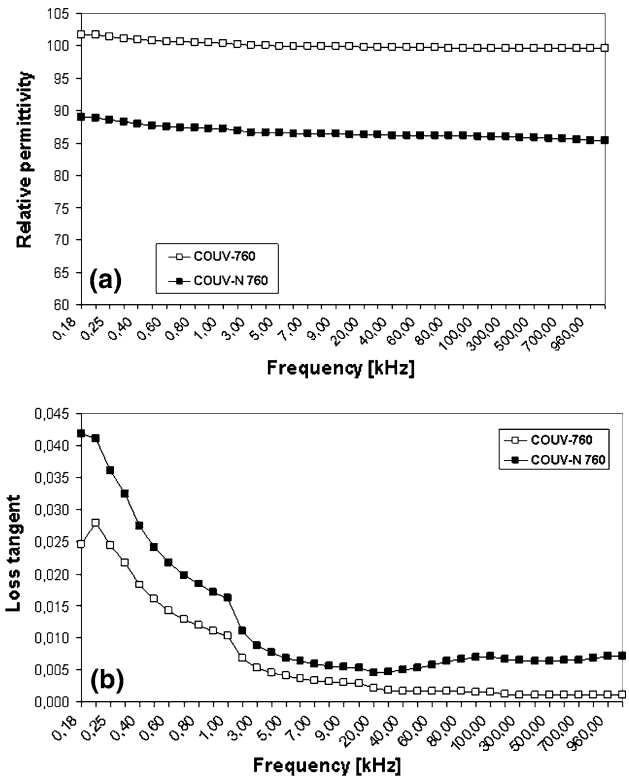

Fig. 10 Relative permittivity (a) and Loss tangent (b) of the argon (COUV) and nitrogen (COUV-N) assisted TiO_2 coatings after annealing at 760 °C

with partly changed microstructures compared to as-sprayed coatings, see Fig. 9, can be evaluated as dielectrics. The dependence of a relative permittivity on frequency (Fig. 10a) and a loss tangent dependence on frequency (Fig. 10b) were measured. Concerning the dielectric response in AC-field, the values of relative permittivity of about 102 and 86 are shown for the Ar-assisted and the N-assisted coating, respectively. Relative permittivity of rutile is anisotropic—in the direction parallel with the tetragonal axis $\varepsilon_r = 173$ and in the perpendicular direction $\varepsilon_r = 89$ (Ref 34). The Ar-assisted coating has higher permittivity at lower losses and also at higher resistivity than the other one. The combination of all those factors indicates a slightly higher degree of re-oxidation in the case of the Ar-assisted coating. It seems to be connected with its lower degree of chemical disorder, as revealed by XPS. After annealing, the Ar-assisted coating seems to approach more closely the TiO_2 stoichiometry than the other one. For a random grain orientation the value of relative permittivity is between 115 and 130. The relative permittivity of anatase is 55 (Ref 34). Both our coatings are between nominal values of anatase and rutile phases because of the expectedly random grain orientation and also the presence of defects like pores and microcracks that need higher temperatures for thermal healing (Ref 36). The loss tangent value of the Ar-assisted coating is in perfect agreement with reported rutile samples [$\tan \delta = 2.3 \times 10^{-3}$ at 1 MHz (Ref 35)].

4. Conclusions

Titanium dioxide powders were sprayed by a WSP gun to form coatings with a photocatalytically active surface. Agglomerated nanometric powder with anatase as the dominant phase was used as a feedstock. Either argon or nitrogen was employed as both powder-feeding and coating-cooling gases. The photocatalytic activity was tested by decomposition of acetone at UV illumination and the nitrogen-assisted sample proved to be the more efficient photocatalyst. The Ar- and N-assisted coatings differ in the quantity of superficial OH groups and interstitial N atoms. Upon irradiation with UV light the OH groups form OH radicals. The OH radical is an important activator of the photocatalytic processes. The acetone decomposition is therefore faster for the N-assisted coating

with more OH groups in its structure. At the same time this coating has higher porosity, which means higher contact surface for the acetone and the UV light. However, from the mechanical viewpoint the other, Ar-assisted, coating is slightly better.

The hydrogen content is higher for the N-assisted coating. The "x" of the as-sprayed TiO_x coating seems to be also influenced by the reactivity of nitrogen: estimations based on XPS results indicate that a reduction of the Ar-coating is about one half of those for the N-coating.

It has also been confirmed in this work that obtaining a coating with the best attainable mechanical performance and with maximal photocatalytic efficiency is an arduous task since these requirements go against each other. Nevertheless, the presented work demonstrates a viable way to make a compromise when producing a coating by the WSP spraying.

Acknowledgments

The work done at IPP ASCR was supported by the Academy of Science of the Czech Republic under project AV0 Z20430508 and the work done at FMP by the research program MSM 0021620834 financed by the Ministry of Education of the Czech Republic. I. Píš thanks also the Grant Agency of the Czech Republic (Grant No. 202/09/H041) for the research support. The authors thank N. Murafa, IIC ASCR, for the HR-TEM micrographs.

References

1. N. Negishi, K. Takeuchi, and T. Ibusuki, The Surface Structure of Titanium Dioxide Thin Film Photocatalyst, *Appl. Surf. Sci.*, 1997, **121**, p 417-420
2. S. Matsuda, H. Hatano, and A. Tsutsumi, Ultrafine Particle Fluidization and Its Application to Photocatalytic NO_x Treatment, *Chem. Eng. J.*, 2001, **82**, p 183-188
3. K. Brinkiene, R. Kezelis, A. Baltusnikas, V. Mecius, and V. Matulioniene, Investigation of the Properties of Plasma Sprayed Titania, *Mater. Sci.*, 2004, **10**, p 345-348
4. F.-L. Toma, G. Bertrand, D. Klein, C. Meunier, and S. Begin, Development of Photocatalytic Active TiO_2 surfaces by Thermal Spraying of Nanopowders, *J. Nanomater.*, 2008, Article ID 384171, doi:10.1155/2008/384171
5. I. Tsuyumoto and H. Uchikawa, Nonstoichiometric Orthorhombic Titanium Oxide, TiO_{2-x} and Its Thermochromic Properties, *Mater. Res. Bull.*, 2004, **39**, p 1737-1744
6. I. Burlacov, J. Jirkovsky, M. Müller, and R.B. Heimann, Induction Plasma-Sprayed Photocatalytically Active Titania Coatings and Their Characterisation by Micro-Raman Spectroscopy, *Surf. Coat. Technol.*, 2006, **201**, p 255-264
7. H. Chen, S.W. Lee, T.H. Kim, and B.Y. Hur, Photocatalytic Decomposition of Benzene with Plasma Sprayed TiO_2-Based Coatings on Foamed Aluminum, *J. Eur. Ceram. Soc.*, 2006, **26**, p 2231-2239
8. T. Kanazawa and A. Ohmori, Behavior of TiO_2 Coating Formation on PET Plate by Plasma Spraying and Evaluation of Coating's Photocatalytic Activity, *Surf. Coat. Technol.*, 2005, **197**, p 45-50
9. Ch. Lee, H. Choi, C. Lee, and H. Kim, Photocatalytic Properties of Nano-Structured TiO_2 Plasma Sprayed Coating, *Surf. Coat. Technol.*, 2003, **173**, p 192-200
10. J. Colmenares-Angulo, S. Zhao, C. Young, and A. Orlov, The Effects of Thermal Spray Technique and Post-Deposition Treatment on the Photocatalytic Activity of TiO_2 Coatings, *Surf. Coat. Technol.*, 2009, **204**, p 423-427
11. M. Bozorgtabar, M. Rahimipour, and M. Salehi, Novel Photocatalytic TiO_2 Coatings Produced by HVOF Thermal Spraying Process, *Mater. Lett.*, 2010, **64**, p 1173-1175
12. S. Kozerski, F.-L. Toma, L. Pawlowski, B. Leupolt, L. Latka, and L.-M. Berger, Suspension Plasma Sprayed TiO_2 Coatings Using Different Injectors and Their Photocatalytic Properties, *Surf. Coat. Technol.*, 2010, **205**, p 980-986
13. P. Ctibor, K. Neufuss, and P. Chraska, Microstructure and Slurry Abrasion Resistance of Plasma Sprayed Titania Coatings, *J. Therm. Spray Technol.*, 2006, **15**(4), p 689-694
14. M.K. Reddy, S.V. Manorama, and A.R. Reddy, Bandgap Studies on Anatase Titanium Dioxide, *Mater. Chem. Phys.*, 2002, **78**, p 239-245
15. L.-M. Berger, C.C. Stahr, S. Saaro, S. Thiele, M. Woydt, and N. Kelling, Dry Sliding Up to 7.5 m/s and 800°C of Thermally Sprayed Coatings of the TiO_2-Cr_2O_3 System and (Ti, Mo)(C, N)-Ni(Co), *Wear*, 2009, **267**, p 954-964
16. I.N. Martyanov, T. Berger, O. Diwald, S. Rodrigues, and K.J. Klabunde, Enhancement of TiO_2 Visible Light Photoactivity Through Accumulation of Defects During Reduction-Oxidation Treatment, *J. Photochem. Photobiol. A*, 2010, **212**, p 135-141
17. T.D. Robert, L.D. Laude, V.M. Geskin, R. Lazzaroni, and R. Gouttebaron, Micro-Raman Spectroscopy Study of Surface Transformations Induced by Excimer Laser Irradiation of TiO_2, *Thin Solid Films*, 2003, **440**, p 268-277
18. C. Giolli, F. Borgioli, A. Credi, A. Di Fabio, A. Fossati, M. Muniz Miranda, S. Parmeggiani, G. Rizzi, A. Scrivani, S. Troglio, A. Tolstoguzov, A. Zoppi, and U. Bardi, Characterization of TiO_2 Coatings Prepared by a Modified Electric Arc-Physical Vapour Deposition System, *Surf. Coat. Technol.*, 2007, **202**, p 13-22
19. V. Krishnan, S. Heislbetz, M.M. Natile, A. Glisenti, and H. Bertagnolli, Influence of Preparation Technique and Iron Doping on the Structure and Reactivity of Mixed Fe-Ti-O Nanocomposites, *Mater. Chem. Phys.*, 2005, **92**, p 394-402
20. M. Vilay, P.V. Ananthapadmanabhan, and K.P. Sreekumar, Evolution of Photo-Catalytic Properties of Reactive Plasma Processed Nano-Crystalline Titanium Dioxide Powder, *Appl. Surf. Sci.*, 2009, **255**, p 9316-9322
21. T.K. Sham and M.S. Lazarus, X-Ray Photoelectron Spectroscopy (XPS) Studies of Clean and Hydrated TiO_2 (Rutile) Surfaces, *Chem. Phys. Lett.*, 1979, **68**(2-3), p 426-432
22. V.V. Atuchin, V.G. Kesler, N.V. Pervukhina, and Z. Zhang, Ti 2p and O1s Core Levels and Chemical Bonding in Titanium-Bearing Oxides, *J. Electron Spectrosc. Relat. Phenom.*, 2006, **152**, p 18-24
23. F.-L. Toma, G. Bertrand, S. Begin, C. Meunier, O. Barres, D. Klein, and C. Coddet, Microstructure and Environmental Functionalities of TiO_2-Supported Photocatalysts Obtained by Suspension Plasma Spraying, *Appl. Catal. B*, 2006, **68**, p 74-84
24. H. Shen, L. Mi, P. Xu, W. Shen, and P.-N. Wang, Visible-Light Photocatalysis of Nitrogen-Doped TiO_2 Nanoparticulate Films Prepared by Low-Energy Ion Implantation, *Appl. Surf. Sci.*, 2007, **253**, p 7024-7028
25. F. Napoli, M. Chiesa, S. Livraghi, E. Giamello, S. Agnoli, G. Granozzi, G. Pacchioni, and C. Di Valentin, The Nitrogen Photoactive Centre in N-Doped Titanium Dioxide Formed Via Interaction of N Atoms with the Solid. Nature and Energy Level of the Species, *Chem. Phys. Lett.*, 2009, **477**, p 135-138
26. T. Chiaramonte, L.P. Cardoso, R.V. Gelamo, F. Fabreguette, M. Sacilotti, M.C. Marco de Lucas, L. Imhoff, S. Bourgeois, Y. Kihn, and M.-J. Casanove, Structural Characterization of TiO_2/TiN_xO_y (d-Doping) Heterostructures on (110) TiO_2 Substrates, *Appl. Surf. Sci.*, 2003, **212-213**, p 661-666
27. F. Dong, W. Zhao, Z. Wu, and S. Guo, Band Structure and Visible Light Photocatalytic Activity of Multi-Type Nitrogen Doped TiO_2 Nanoparticles Prepared by Thermal Decomposition, *J. Hazard. Mater.*, 2009, **162**, p 763-770
28. N. Hosaka, T. Sekiya, M. Fujisawa, Ch. Satoko, and S. Kurita, UV Reflection Spectra of Anatase TiO_2, *J. Electron Spectrosc. Relat. Phenom.*, 1996, **78**, p 75-78

29. J. Ryu, D.-S. Park, B.-D. Hahn, J.-J. Choi, W.-Ha. Yoon, K.-Y. Kim, and H.-S. Yun, Photocatalytic TiO_2 Thin Films by Aerosol-Deposition: From Micron-Sized Particles to Nano-Grained Thin Film at Room Temperature, *Appl. Catal. B*, 2008, **83**, p 1-7
30. L. Wan, J.F. Li, J.Y. Feng, W. Sun, and Z.Q. Mao, Anatase TiO_2 Films with 2.2 eV Band Gap Prepared by Micro-Arc Oxidation, *Mater. Sci. Eng. B*, 2007, **139**, p 216-220
31. D.C. Hurum, A.G. Agrios, S.E. Crist, K.A. Gray, T. Rajh, and M.C. Thurnauer, Probing Reaction Mechanisms in Mixed Phase TiO_2 by EPR, *J. Electron Spectrosc. Relat. Phenom.*, 2006, **150**, p 155-163
32. E. Barajas-Ledesma, M.L. García-Benjume, I. Espitia-Cabrera, M. Ortiz-Gutierez, F.J. Espinoza-Beltran, J. Mostaghimi, and M.E. Contreras-Garcia, Determination of the Band Gap of TiO_2-Al_2O_3 Films as a Function of Processing Parameters, *Mater. Sci. Eng. B*, 2010, **174**, p 71-73
33. V. Nadtochenko, N. Denisov, A. Gorenberg, Y. Kozlov, P. Chubukov, J.A. Rengifo, C. Pulgarin, and J. Kiwi, Correlations for Photocatalytic Activity and Spectral Features of the Absorption Band Edge of TiO_2 Modified by Thiourea, *Appl. Catal. B*, 2009, **91**, p 460-469
34. Gmelins Handbook of Inorganic Chemistry, vol. 41—Titan, Springer, Berlin, 1976, p 426, in German
35. C.T. Dervos, E. Thirios, J. Novacovich, P. Vassiliou, and P. Skafidas, Permittivity Properties of Thermally Reated TiO_2, *Mater. Lett.*, 2004, **58**, p 1502-1507
36. P. Ctibor, P. Boháč, M. Stranyánek, and R. Čtvrtlík, Structure and Mechanical Properties of Plasma Sprayed Coatings of Titania and Alumina, *J. Eur. Ceram. Soc.*, 2006, **26**(16), p 3509-3514